Title

Improved estimates of global terrestrial photosynthesis using information on leaf chlorophyll content

Journal

Global Change Biology, 25(7)

ISSN

1354-1013

Authors

Luo, Xiangzhong
Croft, Holly
Chen, Jing M
et al.

Publication Date

2019-07-01

DOI

10.1111/gcb.14624

Peer reviewed

Improved estimates of global terrestrial photosynthesis using information on leaf chlorophyll content

Xiangzhong Luo[1,2,3] | Holly Croft[1] | Jing M. Chen[1] | Liming He[1] | Trevor F. Keenan[2,3]

[1] Department of Geography and Planning, University of Toronto, Toronto, ON, Canada [2] Climate and Ecosystem Sciences Division, Lawrence Berkeley National Laboratory, Berkeley, California [3] Department of Environmental Science, Policy and Management, University of California, Berkeley, California

Correspondence Jing M. Chen, Department of Geography and Planning, University of Toronto, Toronto, ON, Canada. Email: jing.chen@utoronto.ca

Abstract

The terrestrial biosphere plays a critical role in mitigating climate change by absorbing anthropogenic CO_2 emissions through photosynthesis. The rate of photosynthesis is determined jointly by environmental variables and the intrinsic photosynthetic capacity of plants (i.e. maximum carboxylation rate; V_{cmax}^{25}). A lack of an effective means to derive spatially and temporally explicit V_{cmax}^{25} has long hampered efforts towards estimating global photosynthesis accurately. Recent work suggests that leaf chlorophyll content (Chl_{leaf}) is strongly related to V_{cmax}^{25}, since Chl_{leaf} and V_{cmax}^{25} are both correlated with photosynthetic nitrogen content. We used medium resolution satellite images to derive spatially and temporally explicit Chl_{leaf}, which we then used to parameterize V_{cmax}^{25} within a terrestrial biosphere model. Modelled photosynthesis estimates were evaluated against measured photosynthesis at 124 eddy covariance sites. The inclusion of Chl_{leaf} in a terrestrial biosphere model improved the spatial and temporal variability of photosynthesis estimates, reducing biases at eddy covariance sites by 8% on average, with the largest improvements occurring for croplands (21% bias reduction) and deciduous forests (15% bias reduction). At the global scale, the inclusion of Chl_{leaf} reduced terrestrial photosynthesis estimates by 9 PgC/year and improved the correlations with a reconstructed solar-induced fluorescence product and a gridded photosynthesis product upscaled from tower measurements. We found positive impacts of Chl_{leaf} on modelled photosynthesis for deciduous forests, croplands, grasslands, savannas and wetlands, but mixed impacts for shrublands and evergreen broadleaf forests and negative impacts for evergreen needleleaf forests and mixed forests. Our results highlight the potential of Chl_{leaf} to reduce the uncertainty of global photosynthesis but identify challenges for incorporating Chl_{leaf} in future terrestrial biosphere models.

KEYWORDS: gross primary productivity, leaf chlorophyll content, photosynthetic capacity, remote sensing, solar-induced fluorescence, terrestrial biosphere models

1 INTRODUCTION

The terrestrial biosphere has been a substantial carbon sink over the past half century, absorbing around one third of anthropogenic CO_2 emissions (Keenan & Williams, 2018; Le Quéré et al., 2017). This net carbon sink exists due to a slight difference between carbon uptake through photosynthesis and carbon loss through ecosystem respiration and natural disturbances (i.e. wild fires). The size of individual carbon fluxes is generally one to two orders of magnitude larger than the net carbon sink (Beer et al., 2010; Bond-Lamberty & Thomson, 2010; Sitch et al., 2015), therefore, a small negative change in photosynthesis can easily influence the ability of the land sink to mitigate anthropogenic CO_2 emissions.

Currently, estimates of global photosynthesis (gross primary production; GPP) from state-of-the-art terrestrial biosphere models (TBMs) vary in a wide range from 112 to 169 PgC/year (Baldocchi, Ryu, & Keenan, 2016; Piao et al., 2013), accompanied by substantial discrepancies in estimated trends and variability of GPP (Anav et al., 2015; Li, Ciais, et al., 2018). Much of the uncertainty in GPP is attributed to an inadequate constraint of the maximum leaf carboxylation rate (normalized to 25 degrees; V_{cmax}^{25}) in TBMs (Bonan et al., 2011; Schaefer et al., 2012; Walker et al., 2017). V_{cmax}^{25} is related to the concentration of the photosynthetic enzyme ribulose-1,5-bisphosphate carboxylase/oxygenase (Rubisco) (Farquhar, von Caemmerer, & Berry, 1980) and is known to change over time and space under the influence of a wide range of factors, including leaf ontogeny (Croft et al., 2017), nutrient availability (Walker et al., 2014), seasonality of climatic variables (Misson, Tu, Boniello, & Goldstein, 2006), extreme weather (Zhou et al., 2014) and biodiversity and stand age (Musavi et al., 2017). However, the variability of V_{cmax}^{25} has yet to be fully considered in most currently used TBMs because of the difficulty in obtaining spatially and temporally continuous V_{cmax}^{25} for large-scale simulations from direct observations of V_{cmax}^{25}, which require measurements of leaf photosynthesis under varying CO_2 concentrations (Stinziano et al., 2017; Wullschleger, 1993; Xu & Baldocchi, 2003). Therefore, current TBMs are limited to using fixed V_{cmax}^{25} values specific to plant functional types (PFTs) and empirical scaling functions to partly consider the variation in V_{cmax}^{25} when estimating global photosynthesis (Ryu et al., 2011; Thornton & Zimmermann, 2007).

Previous studies have attempted to derive V_{cmax}^{25} from remotely sensed data, given that the spectrum of the land surface reflectance is influenced by leaf physiology and plant function. Statistical models (i.e. partial least square regression, PLSR) have been used to derive nitrogen content from the surface reflectance spectra for both leaves (Singh, Serbin, McNeil, Kingdon, & Townsend, 2015) and canopies (Dechant, Cuntz, Vohland, Schulz, &

Doktor, 2017). Some studies have adopted similar models to estimate V_{cmax}^{25} of leaves (Barnes et al., 2017; Dechant et al., 2017) and canopies (Serbin et al., 2015), considering that nitrogen content is a strong indicator of V_{cmax}^{25} (Kattge, Knorr, Raddatz, & Wirth, 2009; Walker et al., 2014). However, these empirical models are mostly only reliable in site-specific studies (Wang, Skidmore, Darvishzadeh, & Wang, 2018) and face some challenges when extrapolated to broad spatial scales because of the difficulty in separating the spectral signature of nitrogen, a nonpigment constituent, from overlapping and covarying signatures of other biochemical constituents of vegetation within different landscapes (Kokaly, Asner, Ollinger, Martin, & Wessman, 2009). Solar-induced fluorescence (SIF; 650–800 nm) is another remotely sensed indicator that has been used to derive V_{cmax}^{25} (Zhang et al., 2014; Zhang, Guanter, Joiner, Song, & Guan, 2018), considering the widely reported tight correlation between SIF and leaf photosynthesis (Yang et al., 2017) or GPP (Frankenberg et al., 2011; Guanter et al., 2014; Li, Xiao, & He, 2018). However, the derivation of V_{cmax}^{25} from SIF faces the challenge of separating the impact of canopy structure on GPP from that of leaf physiological traits since the canopy-scale SIF contains information of both (Liu et al., 2018; Yang & van der Tol, 2018).

Chlorophyll is a crucial component of plant photosynthesis machinery, through harvesting photons and transporting electrons to support the production of biochemical energy for the Calvin-Benson cycle (Alton, 2017; Porcar-Castell et al., 2014). Leaf chlorophyll content (Chl_{leaf}), defined as the total chlorophyll *a* and chlorophyll *b* content per one half of the total leaf area (all sided), can act as a proxy for the photosynthetic nitrogen pool, which is also shared by Rubisco (Evans, 1989b; Hikosaka & Terashima, 1996). Recent studies have found linear relationships between Chl_{leaf} and V_{cmax}^{25} for several tree species (Croft et al., 2017) and agricultural crops (Houborg, Cescatti, Migliavacca, & Kustas, 2013; Houborg, McCabe, Cescatti, & Gitelson, 2015), and the integration of these Chl_{leaf}-V_{cmax}^{25} relationships into TBMs has been reported to reduce errors of estimated GPP at a cropland site (Houborg et al., 2013) and a forest site (Luo, Croft, et al., 2018). Since the Chl_{leaf}-V_{cmax}^{25} relationship is known to change with the light environment within a canopy (Evans, 1989a; Poorter, Kwant, Hernández, & Medina, 2000), an updated two-leaf scheme has been developed to account for the difference between the Chl_{leaf}-V_{cmax}^{25} relationship for sunlit leaves and that for shaded leaves in TBMs (Luo, Croft, et al., 2018). It is also argued that Chl_{leaf} serves as a better proxy for V_{cmax}^{25} than the commonly used area-based leaf nitrogen content (N_{area}), because N_{area} includes the nitrogen for both photosynthetic and nonphotosynthetic components (i.e. structural development), and the nonphotosynthetic component can complicate the apparent N_{area}-V_{cmax}^{25} relationships (Croft et

al., 2017). Chl_{leaf} effectively removes the influence of nonphotosynthetic nitrogen and only reflects the changes in the photosynthetically active nitrogen pool (Croft et al., 2017).

Recent developments in using physically based approaches to estimate Chl_{leaf} from satellite data (Croft, Chen, Zhang, & Simic, 2013; Houborg, McCabe, Cescatti, Gao, et al., 2015; Zhang, Chen, Miller, & Noland, 2008) have made it possible to estimate globally continuous Vc_{max}^{25}. These physically based approaches used established radiative transfer theories to downscale the remotely sensed canopy reflectance to leaf reflectance (Kuusk, 2018) and then use the leaf reflectance in a leaf optical model (Jacquemoud & Ustin, 2001) to estimate Chl_{leaf}. This can remove the effect of background reflectance, multiple scattering and the bidirectional reflectance distribution function (BRDF) effects of a canopy to distil the spectral signal of Chl_{leaf} only.

Here, we examine the potential of using satellite-derived Chl_{leaf} to estimate temporally and spatially explicit Vc_{max}^{25} across a diverse array of sites around the globe. To do so, we applied a two-step physically based approach (Croft et al., 2013; Simic, Chen, & Noland, 2011; Zhang et al., 2008) to derive Chl_{leaf} at 124 eddy covariance sites (555 site-years) from the FLUXNET2015 tier 1 data set (Baldocchi, 2008; Pastorello et al., 2017), and modelled the GPP of these sites with and without Chl_{leaf}-based Vc_{max}^{25}. We examined the effects of the inclusion of Chl_{leaf} in GPP modelling for each of the nine PFTs and further estimated global GPP. We compared the global GPP against a reconstructed SIF product (Gentine & Alemohammad, 2018), a remote sensing-based GPP product (Zhao, Heinsch, Nemani, & Running, 2005) and a global GPP product upscaled from eddy covariance measurements (Jung et al., 2017).

2 MATERIALS AND METHODS

2.1 Flux, meteorological and satellite data

FLUXNET2015 is the latest effort to refine the flux measurements from eddy covariance towers of different regional networks and publish the data in a standard format (Pastorello et al., 2017). It provides gap-filled GPP estimates and their concurrent meteorological records for over 200 sites. In this study, we used the FLUXNET2015 tier 1 data set released in November 2016. We selected 124 sites (555 site-years) (Supporting Information, section 1) based on the availability of the MEdium Resolution Imaging Spectrometer (MERIS) satellite data that were used for the leaf chlorophyll content (Chl_{leaf}) derivation. We chose to use GPP partitioned from Net Ecosystem Exchange (NEE) using a night-time method (NT) with variable u* threshold (VUT) for each year. NT uses only night-time data to parameterize a respiration model that is then applied to the whole data set to estimate ecosystem respiration and then calculate GPP (Reichstein et al., 2005). Many versions of the GPP records were created by using different percentiles of u*. Among those GPP versions, we regarded GPP_NT_VUT_REF as the reference GPP, which was

estimated by using the VUT and the original u* values. The observational uncertainty of GPP was provided by the field GPP_NT_VUT_SE in the data set.

Half-hourly and hourly meteorological records in the FLUXNET2015 data set were used to drive a TBM to estimate GPP. Gap-filled solar radiation (SW_IN_F), air temperature (TA_F), vapour pressure deficit (VPD_F), precipitation (P_F) and wind speed (WS_F) were selected as the forcing variables for the TBM, to allow the TBM to produce continuous hourly results. For GPP modelling at the global scale, we used MERRA-2 (Modern-Era Retrospective Analysis for Research and Applications, Version 2) data from Goddard Space Flight Center, NASA as the climate forcing to drive the TBM (He et al., 2018).

Leaf area index (LAI) series are required to drive the TBM and derive Chl_{leaf}. We selected the Copernicus Global Land Service GEOV1 LAI product derived from SPOT-VEGETATION satellite, which has a global coverage of LAI from 1999 to 2014, at 10 day temporal intervals and a spatial resolution of 1 km (Baret et al., 2013). We used the Locally Adjusted Cubic-spline Capping (LACC) method (Chen, Deng, & Chen, 2006) to interpolate and smooth the discontinuous LAI into daily LAI series.

Clumping index (Ω, or CI) describes the nonrandomness of the leaf distribution in the canopy (Chen, Rich, Gower, Norman, & Plummer, 1997). It is a key parameter to drive the canopy radiation transfer module in both the TBM and the Chl_{leaf} derivation algorithm. Site-specific CI values were obtained from a global foliage clumping index map produced from the MODIS BRDF products (He, Chen, Pisek, Schaaf, & Strahler, 2012). The map has a resolution of 500 m, which is comparable to the size of regular tower footprints.

MEdium Resolution Imaging Spectrometer (MERIS) full resolution surface reflectance (SR) product was selected for deriving global Chl_{leaf} maps. MERIS SR data were chosen due to the presence of chlorophyll-sensitive red-edge bands, fine temporal resolution (every 2–3 days), medium spatial resolution (300 m) and high radiometric accuracy (Curran & Steele, 2005). The SR product was produced as a 7 day temporal synthesis from images collected at the original 2–3 day revisit frequency (Rast, Bezy, & Bruzzi, 1999). The MERIS surface reflectance series were produced by a series of preprocessing steps, including radiometric, geometric and BRDF correction, pixel identification and atmospheric correction with aerosol retrieval. There are 13 bands (spectral resolution ~=10 nm) in the visible, red-edge and near-infrared bands sampled in the reflectance data set. MERIS covers the complete years from 2003 to 2011. We extracted the surface reflectance in all bands at every flux tower site as the input for the Chl_{leaf} derivation algorithm. In order to retain enough sampling points to detect the seasonal patterns of Chl_{leaf}, only the site-years that have more than 10 MERIS surface reflectance records were considered in this study.

Solar-induced fluorescence (SIF). We used a recently released reconstructed SIF product (Gentine & Alemohammad, 2018) to evaluate the estimates of global photosynthesis. The reconstructed SIF (RSIF) is the product of photosynthetic active radiation (PAR) estimated by BESS (Ryu et al., 2011) and the reconstructed Global Ozone Monitoring-2 (GOME-2) SIF normalized by solar zenith angle (SZA), while the reconstructed GOME-2 SIF normalized by SZA was produced by a neural network trained on the original GOME-2 SIF normalized by SZA (Joiner et al., 2011) with the input of MODIS surface reflectance. This RSIF product exhibits much higher seasonal and interannual correlation than the original SIF when compared with eddy covariance estimates of GPP and two reference global GPP products (Gentine & Alemohammad, 2018). It has a more continuous coverage over time and space and a higher signal-to-noise ratio than the original SIF. We downloaded the monthly RSIF at 0.5°
from https://gentinelab.eee.columbia.edu/content/datasets. While using RSIF as a proxy for GPP in this study, we acknowledged that the strong correlation between SIF and GPP is largely explained by the dependence of both absorbed photosynthetic active radiation (APAR) (Zhang et al., 2016), and a recent study even suggested that SIF is more likely a proxy for APAR than for photosynthesis at a rice paddy (Yang et al., 2018).

FLUXCOM global carbon flux data set. FLUXCOM (Jung et al., 2017) produced global GPP estimates by upscaling site-level GPP from 224 flux tower sites using three machine learning algorithms: Random forests (RF), Artificial Neural Networks (ANN) and Multivariate Adaptive Regression Splines (MARS). Each machine learning algorithm was trained on daily fluxes using 11 inputs including site-level meteorological and remote sensing observations. After obtaining the trained algorithm, gridded climatic variables (CRU-NCEP v6) and satellite observations from MODIS were used to produce the gridded carbon flux estimations. We downloaded the monthly GPP estimation at 0.5° from www.bgc-jena.mpg.de/geodb/projects/Data.php.

MODIS GPP. We used MODIS GPP product (MOD17 collection 55) released by the Numerical Terradynamic Simulation Group (NTSG) at the University of Montana. The collection 55 GPP rectifies the underestimation of GPP incurred by cloud-contaminated pixels in the near-real-time MODIS GPP product (MOD17 collection 5) and was recommend for ecological studies (Zhao et al., 2005). MODIS GPP is provided at a monthly step and 0.5° resolution (http://files.ntsg.umt.edu/data/NTSG_Products/).

Plant Functional Types (PFTs). Nine major PFTs were studied, including: croplands (CRO), deciduous broadleaf forests (DBF), evergreen broadleaf forests (EBF), evergreen needleleaf forests (ENF), grasslands (GRA), savannas and woody savannas (SAV), shrublands (SH) and wetlands (WET). For eddy covariance towers, their PFTs types were provided in metadata of the FLUXNET data set (Supporting Information, section 1). For the global-scale study, we used the PFTs classified by the MODIS Land Cover maps (Friedl et al., 2010) curated at 0.5°. For each 0.5° grid cell, we used the PFT

that was most prevalent during the period 2000–2012. FLUXNET metadata and MODIS Land Cover maps both adopted the vegetation classification protocol of the International Geosphere-Biosphere Programme (IGBP) which does not include a C4 class.

2.2 Derivation of global Chl_{leaf}

Global Chl_{leaf} maps were derived from MERIS surface reflectance, according to the procedure outlined in Croft et al. (), using a two-step process-based algorithm. The first step was to retrieve leaf reflectance spectra from satellite-derived canopy reflectance spectra through the inversion of canopy radiative transfer models. The second step was to use the retrieved leaf reflectance spectra from step 1 to estimate Chl_{leaf} by inverting a leaf radiative transfer model. For the first step, two canopy radiative transfer models were selected, according to the structural characteristics of the vegetation present. For spatially 'clumped' vegetation types (i.e. deciduous and coniferous trees, shrubs) we selected the 4-Scale geometrical-optical model (Chen & Leblanc, 1997). The 4-Scale model simulates the BRDF based on the canopy architecture described at four scales: (a) vegetation grouping, (b) crown geometry, (c) branches and (d) foliage elements. A plant crown is, therefore, represented as a complex medium, where mutual scattering occurs between shoots or leaves. The 4-Scale model calculates canopy reflectance (ρ) as a linear summation of four components:

$$\rho = \rho_{PT}F_{PT} + \rho_{ZT}F_{ZT} + \rho_{PG}F_{PG} + \rho_{ZG}F_{ZG} \quad (1)$$

where the sunlit vegetation (ρ_{PT}), shaded vegetation (ρ_{ZT}), sunlit ground (ρ_{PG}) and shaded ground (ρ_{ZG}), and F_{PT}, F_{PG}, F_{PG} and F_{ZT} represent the probability of viewing each component respectively. To derive leaf reflectance (ρ_L) from sunlit crown reflectance (ρ_{PT}), the enhancement of both sunlit and shaded reflectance due to multiple scattering is accounted for using a multiple scattering factor (M factor) (Croft et al., 2013; Simic et al., 2011; Zhang et al., 2008). For homogenous canopies, such as grassland and cropland species, where the distribution of foliage approaches randomness, we used the scattering by arbitrary inclined leaves (SAIL) model (Verhoef, 1984). Turbid medium models such as SAIL assume that the canopy is composed of homogeneous, horizontal layers of Lambertian scatters randomly distributed in space. SAIL is based on the following differential equations: (a) diffuse incoming flux, (b) diffuse outgoing flux, (c) direct solar flux and (d) direct radiant flux in the direction of the sensor. Both canopy reflectance models were inverted using a lookup table (LUT) approach, selected to optimize computational resources and reduce problems associated with local minima (Croft et al.,).

In the second step, Chl_{leaf} was retrieved using the PROSPECT leaf radiative transfer model (Jacquemoud & Baret, 1990) from the modelled leaf reflectance that was derived in step 1. In PROSPECT-5, leaf reflectance and transmittance (400–2,500 nm) are defined as a function of six parameters: structure parameter (N), chlorophyll (a + b) concentration (C_{ab}), carotenoid

content (Car), brown pigment (C_b), dry matter (C_m) and equivalent water thickness (C_w). This two-step approach has been successfully validated over various sites and biomes (Croft et al., 2013; Croft, Chen, Zhang, et al., 2015; Simic et al., 2011; Zhang et al., 2008). Chl_{leaf} derived from the weekly MERIS reflectance observations was then interpolated to daily steps using the LACC method (Chen et al., 2006). Modelled Chl_{leaf} showed a strong relationship with 248 ground measurements collected from 29 globally distributed sites. The relationship has $R^2 = 0.47$ ($p < 0.001$) and RMSE = 10.8 μg/cm^2 (Croft et al.,) (Supporting Information, section 2).

2.3 Conversion of Chl_{leaf} into Vc_{max}^{25}

Several linear equations were used to translate the daily Chl_{leaf} into Vc_{max}^{25} (Table 1). The Vc_{max}^{25}-Chl_{leaf} relationships used for DBF, ENF, MF, SAV, WET were based on a recent work (Croft et al., 2017), who built a single and significant linear relationship across four deciduous broadleaf tree species through direct measurements of Chl_{leaf} and Vc_{max}^{25}. The Vc_{max}^{25}-Chl_{leaf} relationships used for CRO were based on the approach developed by Houborg, McCabe, Cescatti, and Gitelson (2015), who used a mechanistic framework to build an equation to link Chl_{leaf} and Vc_{max}^{25} via area-based leaf total nitrogen content (N_{area}), in which a single equation was developed for croplands. This relationship was also applied to another herbaceous type (GRA) in this study. We then applied a similar method to build Vc_{max}^{25}-Chl_{leaf} equations for EBF and SH, using a comprehensive Vc_{max}^{25}-N_{area} database (Kattge et al., 2009) and a constant ratio between Chl_{leaf} and N_{area} (Evans, 1989b) (Table 1).

TABLE 1 Linear regression equations used to derive Vc_{max}^{25} from Chl_{leaf} ($Vc_{max}^{25} = a \times Chl_{leaf} + b$)

Plant functional types	a (μmol/m^2/s per μg/cm^2)	b (μmol/m^2/s)	Reference
DBF, ENF, MF, SAV, WET	1.3	3.72	Croft et al., 2017
CRO, GRA	1.98	12.5	Houborg, McCabe, Cescatti, & Gitelson, 2015
SH	0.95	14.71	Kattge et al., 2009 and Evans, 1989b
EBF	0.66	6.99	

CRO, croplands; DBF, deciduous broadleaf forests; ENF, evergreen needleleaf forests; GRA, grasslands; MF, mixed forests; SAV, savannas; SH, shrublands; WET, wetlands.

2.4 Modelling GPP using Chl_{leaf}

The TBM used in this study is the Boreal Ecosystem Productivity Simulator (BEPS), which is a two-leaf enzyme kinetic model that has been intensively used to simulate carbon and water fluxes across different biomes (Gonsamo et al., 2013; Wang et al., 2004). It has participated in several cross-model validation studies and been proved to be one of the better performing models for GPP simulations (Grant et al., 2006; Schaefer et al., 2012).

Parameterization of BEPS was demonstrated in detail in previous studies (Chen, Liu, Cihlar, & Goulden, 1999; He et al., 2017; Luo, Chen, et al., 2018). A recent study has upgraded BEPS to integrate Chl_{leaf} (a.k.a. BEPS-Chl_{leaf}) in modelling fluxes in a deciduous broadleaf forest (Luo, Croft, et al., 2018).

Hourly meteorological variables (i.e. solar radiation, temperature, VPD, precipitation and wind speed) are the inputs for BEPS. The solar radiation and leaf temperature are separately calculated for sunlit and shaded leaves through a two-leaf scheme using LAI and CI (Chen et al., 1999). Leaf-level photosynthesis is then obtained from the embedded Farquhar biochemical model with the input of leaf traits.

Three cases were studied depending on the types of Vc_{max}^{25} used in BEPS: (a) BEPS-TRY used constant Vc_{max}^{25} provided by the TRY database (Kattge et al., 2009); (b) BEPS-Chl_{leaf} used daily Chl_{leaf}-based Vc_{max}^{25}; (c) BEPS-Chl_{avg} used the average of daily Chl_{leaf}-based Vc_{max}^{25}.

After using the biochemical model to calculate leaf photosynthesis, stomatal conductance g_s is in turn derived from the Ball–Woodrow–Berry equation and used in the Penman–Monteith model to get leaf transpiration. In feedback, the changes in leaf energy budget modulate the leaf temperature and adjust the photosynthesis rate (Supporting Information, section 3).

After the leaf-level calculation, canopy-scale photosynthesis and transpiration are acquired by multiplying the leaf-level fluxes by the corresponding sunlit and shaded LAI through the two-leaf scheme. Soil texture is prescribed for each site using a global map (https://www.soilgrids.org/) to quantify the hydrological and thermal properties of soil and to simulate soil water content. We apply a linear soil stress factor derived from multilayer soil water content to simulate the stomatal response to possible droughts (Supporting Information, section 3).

Statistical analysis. We used squared Pearson correlation coefficient (r^2), accumulated absolute bias (AAB) and root mean square error (RMSE) to evaluate the performance of models.

AAB was used to quantify the sum of daily GPP biases in a year, avoiding the potential offset of positive and negative daily biases:

$$\mathrm{AAB} = \sum_{i=1}^{n} |A_i - B_i| \quad (2)$$

where n is the size of data population, A_i is the estimate and B_i is the observation.

3 RESULTS

Our satellite-derived estimates of Chl_{leaf} show different seasonal patterns for different PFTs (Figure 1). Chl_{leaf} of DBF, ENF, SAV and WET mostly varied in

range from approximately 5 to 70 μg/cm^2 across a year with a single peak in the growing season; Chl_{leaf} of CRO, MF and SH varied in a similar range showing two or more peaks; Chl_{leaf} of EBF and GRA demonstrated less seasonal variability with the Chl_{leaf} of EBF centred around 67 μg/cm^2 and the Chl_{leaf} of GRA centred around 29 μg/cm^2. There were considerable intersite variations in Chl_{leaf}, as we found the Chl_{leaf} difference between the top quartile sites and the bottom quartile sites for each PFT ranged from 13 μg/cm^2 to 40 μg/cm^2 (Figure 1). We also noticed that there were temporal discrepancies shown between the development of LAI and that of Chl_{leaf} for some PFTs (Figure 1): for DBF and CRO, the peak of Chl_{leaf} appeared 4–5 weeks later than the peak of LAI, and LAI tended to change more dramatically than Chl_{leaf} during a short time frame (i.e. during budburst and leaf fall); for GRA, Chl_{leaf} was relatively stable in contrast to the clear seasonal pattern of LAI; for ENF and SH, Chl_{leaf} showed multiple peaks in a year while LAI only peaked once.

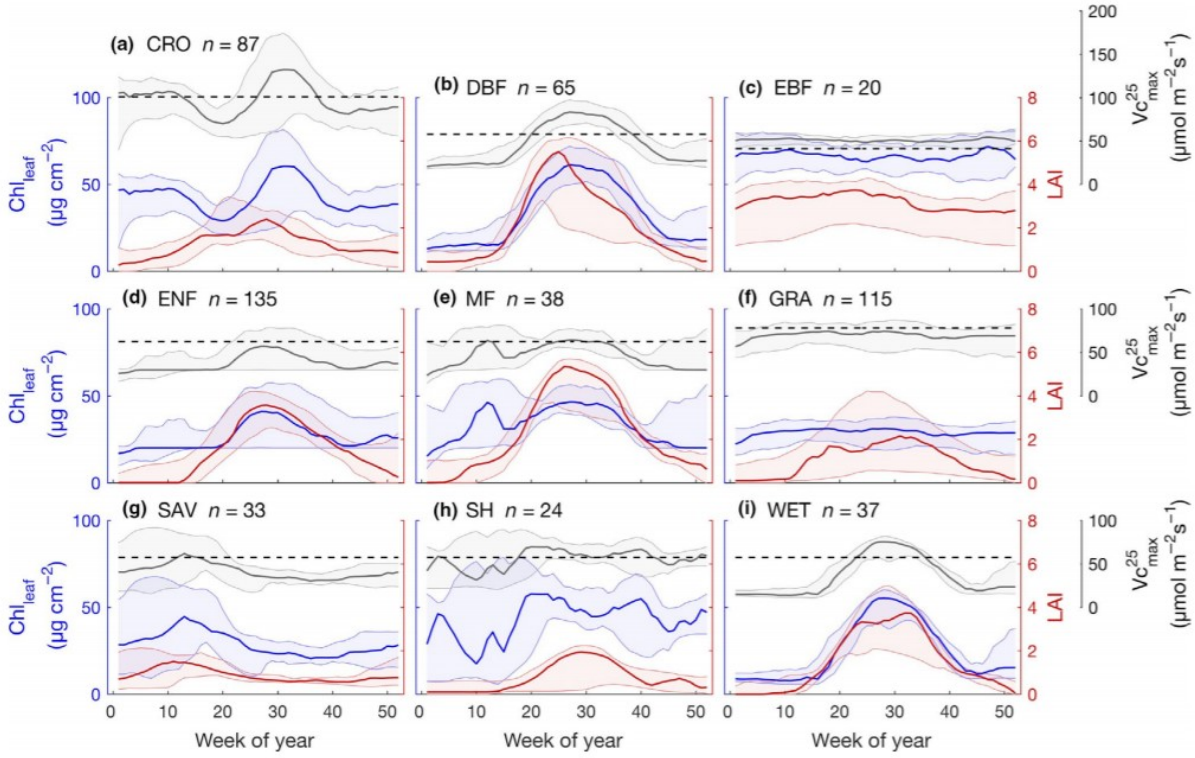

Figure 1. Seasonal dynamics of Chl_{leaf} (blue), LAI (red) and Chl_{leaf}-based Vc_{max}^{25} (solid black) for nine plant functional types (a–i). The plant functional types are croplands (CRO), deciduous broadleaf forests (DBF), evergreen broadleaf forests (EBF), evergreen needleleaf forests (ENF), mixed forests (MF), grasslands (GRA), savannas (SAV), shrublands (SH) and wetlands (WET). The dash lines (black) indicate the constant Vc_{max}^{25} based on the TRY database. *n* indicates the number of site-years for each plant functional type (PFT). The shadings indicate the spatial variations among site-years. In each panel, the solid line is the median of a variable for the group of site-years in a PFT, upper and lower boundaries refer to 75% and 25% percentiles of the variable respectively

We calculated V_{cmax}^{25} from Chl_{leaf} using the PFT-specific equations that we compiled in Table 1. Chl_{leaf}-based V_{cmax}^{25} followed the pattern of Chl_{leaf} across the year (Figure 1). Chl_{leaf}-based V_{cmax}^{25} varied seasonally and spatially in a range between 10 and 80 μmol $m^{-2}s^{-1}$ for most PFTs except for CRO where the Chl_{leaf}-based V_{cmax}^{25} varied between 40 and 175 μmol $m^{-2}s^{-1}$. In comparison with V_{cmax}^{25} from the TRY database, we found that the TRY-based V_{cmax}^{25} were around the annual mean of Chl_{leaf}-based V_{cmax}^{25} for CRO, DBF, SH and WET, and the TRY-based V_{cmax}^{25} generally were larger than their Chl_{leaf}-based V_{cmax}^{25} for ENF, MF, GRA and SAV and vice versa for EBF.

We further used an established two-leaf enzyme kinetic TBM—the Boreal Ecosystem Productivity Simulator (BEPS) to estimate GPP using either Chl_{leaf}-based V_{cmax}^{25} (BEPS-Chl_{leaf}) or TRY-based V_{cmax}^{25} (BEPS-TRY) (see Material and Methods). While BEPS-TRY only used LAI to describe the variability of vegetation status, BEPS-Chl_{leaf} considered both the variabilities of LAI and Chl_{leaf} in the estimation of GPP. The bias of estimated GPP from BEPS-Chl_{leaf} was much smaller, showing seasonal biases closer to zero in all weeks for all PFTs except for EBF and ENF (Figure 2). In spring and autumn, Chl_{leaf} reduced the overestimation of GPP for CRO, DBF, GRA and WET and the underestimation for SAV; in summer, Chl_{leaf} reduced the overestimation of GPP for CRO, GRA and SH and the underestimation for DBF, MF and WET.

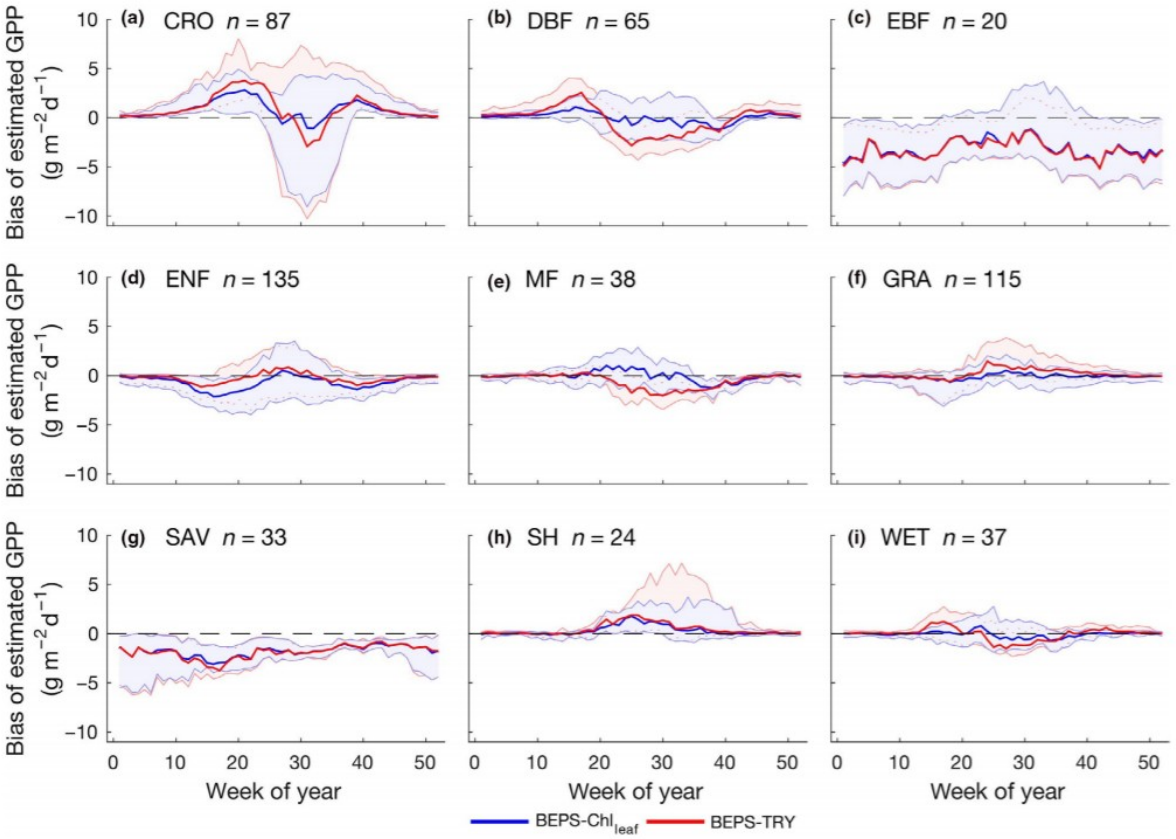

Figure 2. Temporal patterns of the bias of gross primary production estimated by BEPS-Chl_{leaf} (blue) and BEPS-TRY (red) for nine plant functional types (a–i). The plant functional types are croplands (CRO), deciduous broadleaf forests (DBF), evergreen broadleaf forests (EBF), evergreen needleleaf forests (ENF), mixed forests (MF), grasslands (GRA), savannas (SAV), shrublands (SH) and wetlands (WET). *n* indicates the number of sites for each plant functional type. The shadings indicate the spatial variations among site-years. In each panel, the solid line is the median of a variable for the group of site-years in a PFT, upper and lower boundaries refer to 75% and 25% percentiles of the variable respectively

The results above showed that the inclusion of Chl_{leaf} can reduce the spatial and temporal biases in GPP in some cases (Figure 2). To separate the impacts of spatial and temporal variations of Chl_{leaf} on estimated GPP, we added the GPP estimates from BEPS-Chl_{avg} to specifically evaluate the impact of the spatial variation of Chl_{leaf} on GPP estimates, and then evaluated the impact of the temporal variation of Chl_{leaf} based on the difference between BEPS-Chl_{leaf} and BEPS-Chl_{avg} (Figure 3).

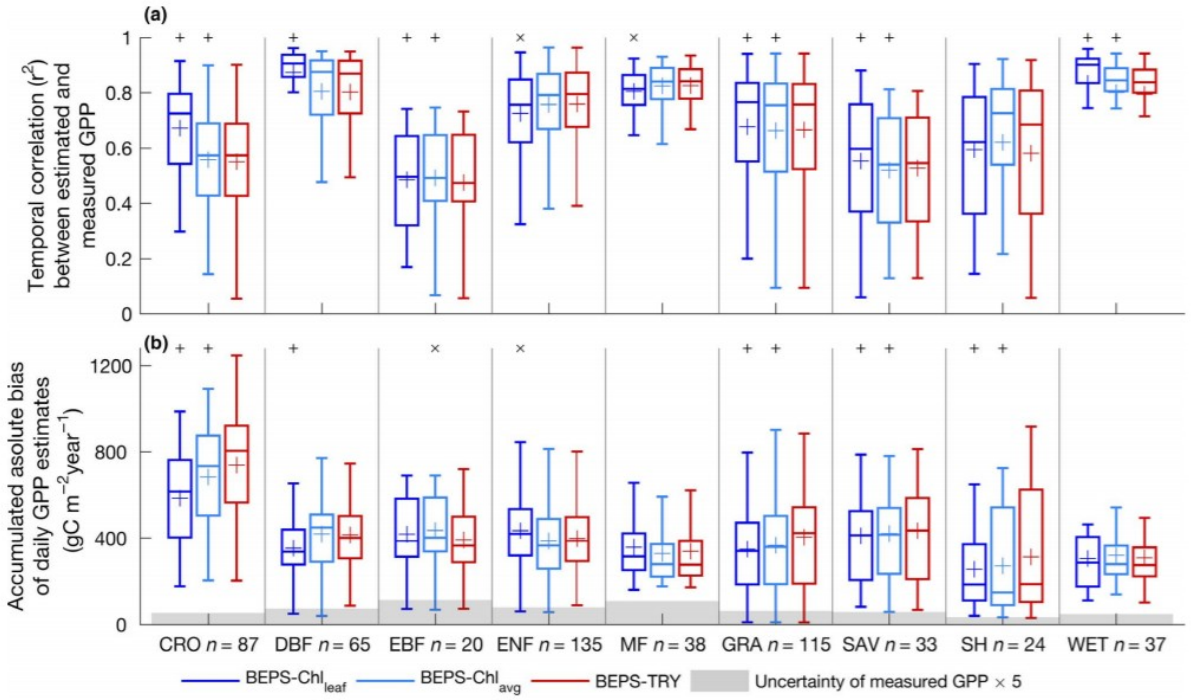

Figure 3. Comparison of daily gross primary production (GPP) estimated by BEPS-Chl$_{leaf}$, BEPS-Chl$_{avg}$ or BEPS-TRY and measured daily GPP for 555 site-years categorized by PFTs. (a) r^2 between the estimated and the measured GPP; (b) accumulated absolute bias (AAB) of the estimated GPP. "+" indicates that BEPS-Chl$_{leaf}$ or BEPS-Chl$_{avg}$ significantly improved GPP estimates compared to those of BEPS-TRY (student's t test, $p < 0.05$) and "x" suggests BEPS-Chl$_{leaf}$ or BEPS-Chl$_{avg}$ results were significantly inferior to those of BEPS-TRY (student's t test, $p < 0.05$). Uncertainty of measured GPP (see Material and Methods) was multiplied by 5 to improve the visibility of shadings in the figure. Acronyms for PFTs are CRO (croplands), DBF (deciduous broadleaf forests), EBF (evergreen broadleaf forests), ENF (evergreen needleleaf forests), MF (mixed forests), GRA (grasslands), SAV (savannas), SH (shrublands) and WET (wetlands)

We found that the temporal correlation (r^2) between daily GPP estimates and measurements was improved from 0.67 ± 0.23 to 0.70 ± 0.22 after the inclusion of Chl$_{leaf}$ (Figure 3a). All PFTs except SH showed significant changes in r^2 (student's t test, $p < 0.05$) after the inclusion of Chl$_{leaf}$. The r^2 for CRO, DBF and WET were improved the most from 0.55 ± 0.19, 0.80 ± 0.17 and 0.79 ± 0.17 to 0.67 ± 0.17, 0.87 ± 0.12 and 0.83 ± 0.18 respectively. In contrast, the r^2 for EBF, ENF and MF decreased slightly. The inclusion of Chl$_{avg}$ fell short of improving the temporal correlation for most PFTs, though some PFTs like CRO, GRA, SAV and WET demonstrated significant (student's t test, $p < 0.05$) but slight increases in r^2.

The accumulated absolute bias (AAB) of GPP decreased by 4% from 551 ± 303 to 527 ± 286 gC m^{-2} yr^{-1} after adding Chl$_{avg}$ to BEPS, and decreased by 8% to 507 ± 261 gC m^{-2} yr^{-1} after adding Chl$_{leaf}$ (Figure 3b). By using BEPS-Chl$_{leaf}$, CRO, DBF, GRA, SAV and SH demonstrated 21%, 15%, 13%, 6% and 19% of AAB reduction respectively (student's t test, $p < 0.05$). But we also noticed a slight 9% increase in AAB for ENF. Meanwhile, BEPS-Chl$_{avg}$ demonstrated similar reductions in the AAB of GPP, only to a smaller degree than those using Chl$_{leaf}$: CRO, GRA, SAV and SH showed a significant

(student's *t* test, $p < 0.05$) decrease in AAB of 8%, 9%, 3% and 13% respectively. Considering the average AAB reductions across site-years were 4% for BEPS-Chl_{avg} and 8% for BEPS-Chl_{leaf}, we found that the spatial variation and temporal variation of Chl_{leaf} contributed equally to the improvement of GPP estimates.

The reductions of daily GPP biases accumulated and led to the improvement of GPP estimates at the annual scale. We found that the spatial correlation (r^2) between estimated and measured annual GPP increased by 5% and RMSE reduced by 21% after the inclusion of Chl_{avg} in BEPS (Figure 4a,b). BEPS-Chl_{leaf} further improved the estimates of GPP on top of BEPS-Chl_{avg}, increasing r^2 by 14% and reducing RMSE by 28% compared to BEPS-TRY (Figure 4a,c). Therefore, both the spatial and temporal variations in Chl_{leaf} improved GPP estimates. The RMSE reduction for annual GPP estimates (28%) appeared more substantial than the reduction of AAB for daily GPP estimates (8%), because the calculation of the former favoured those sites with larger changes in GPP estimates (Figure 4) while the later evaluated the percentage changes of all site-years equally (Figure 3).

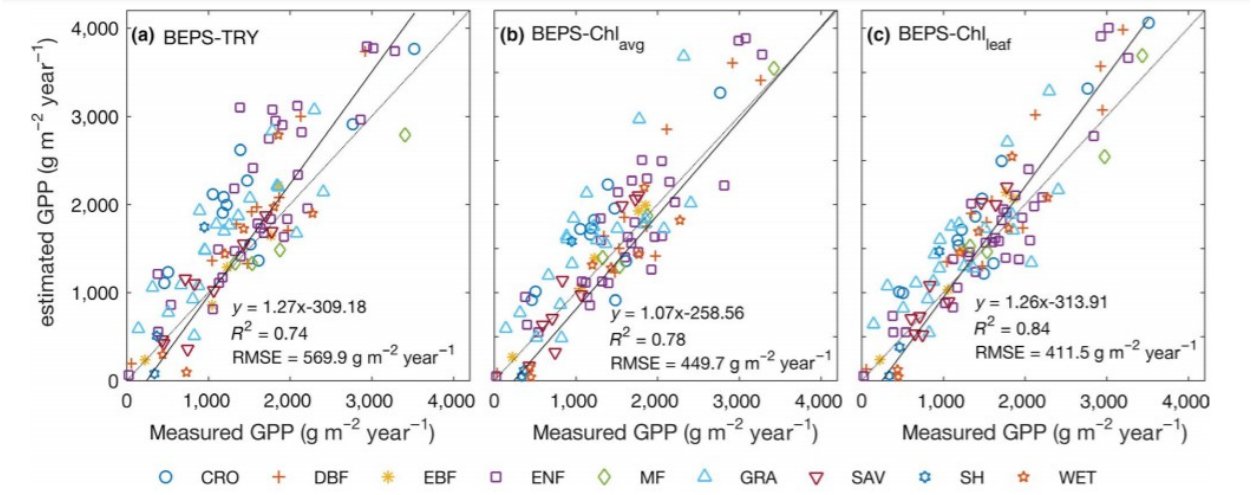

Figure 4. Correlation between measured and estimated annual gross primary production (GPP) of 124 eddy covariance sites. GPP are estimated from (a) BEPS-TRY, (b) BEPS-Chl_{avg} and (c) BEPS-Chl_{leaf}

The global GPP simulated by BEPS-Chl_{leaf} and BEPS-TRY was 121 PgC and 130 PgC in 2011 respectively (Figure 5, Figure S3). The inclusion of Chl_{leaf} in BEPS brought about a 7% decrease of total global GPP, resulting from smaller GPP in the Northern Hemisphere but larger GPP in tropics and the Southern Hemisphere (Figure 5b). Around 40% of the vegetated surface GPP estimates changed more than 200 g m^{-2} per year after the inclusion of Chl_{leaf}, and over 10% of the vegetated surface showed a GPP change larger than 500 g m^{-2} per year.

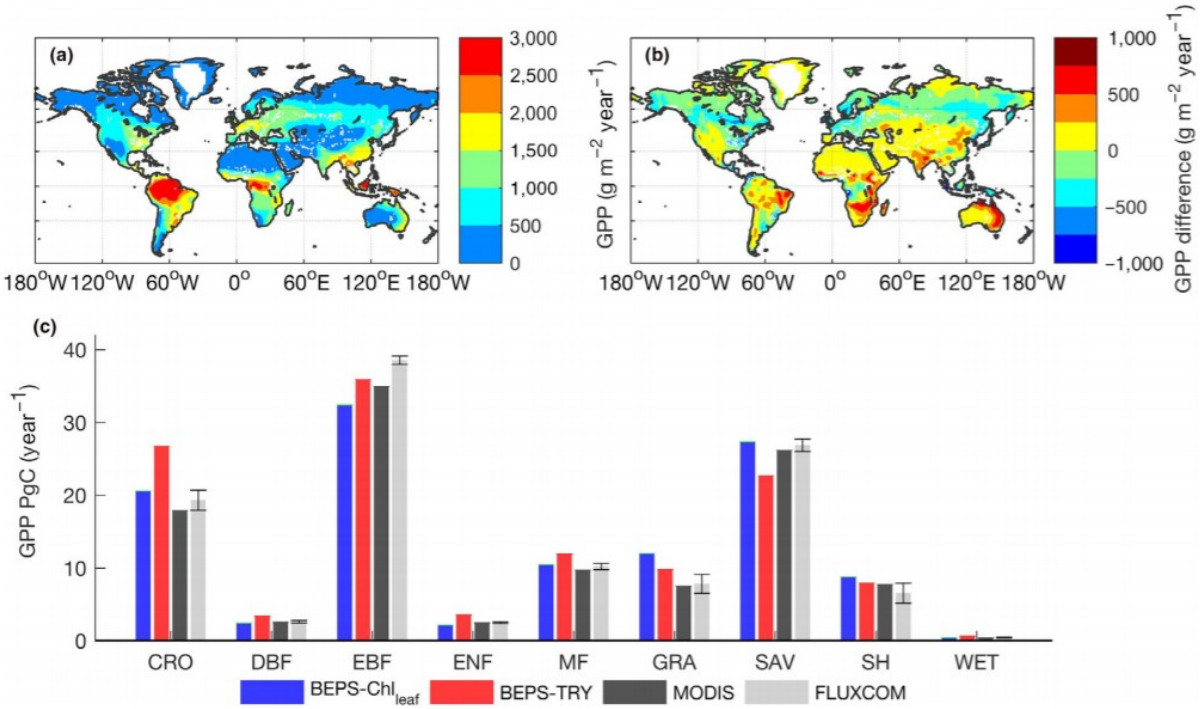

Figure 5. Global gross primary production (GPP) estimated by BEPS-Chl_{leaf} and its comparison with other products. (a) spatial distribution of global GPP estimated by BEPS-Chl_{leaf}; (b) difference between GPP estimated by BEPS-Chl_{leaf} and BEPS-TRY; (c) PFT-specific GPP estimates from BEPS-Chl_{leaf}, BEPS-TRY, MODIS and FLUXCOM. Acronyms for PFTs are CRO (croplands), DBF (deciduous broadleaf forests), EBF (evergreen broadleaf forests), ENF (evergreen needleleaf forests), MF (mixed forests), GRA (grasslands), SAV (savannas), SH (shrublands) and WET (wetlands)

Compared to BEPS-TRY, BEPS-Chl_{leaf} reduced the annual GPP estimates by 6.1 Pg for CRO, 3.4 Pg for EBF and around 1 Pg for each of DBF, ENF and MF. Chl_{leaf} increased the annual GPP estimates of SAV, GRA and SH by 4.7 Pg, 2.1 Pg and 0.9 Pg respectively (Figure 4c). Compared to other widely used global GPP data sets in 2011, the global GPP estimated by BEPS-Chl_{leaf} was larger than MODIS GPP product (113 PgC) and close to the ensemble mean of GPP upscaled from eddy covariance measurements (FLUXCOM; 122 ± 8 PgC).

BEPS-Chl_{leaf} outperformed BEPS-TRY in simulating the variability of global GPP, based on the correlations between estimated annual GPP and RSIF or FLUXCOM GPP (Figure 6). The r^2 between RSIF and estimated GPP increased 0.1 after using Chl_{leaf} in BEPS, while the r^2 between FLUXCOM GPP and estimated GPP increased 0.02. The RMSE between FLUXCOM GPP and estimated GPP also decreased by 5% after the inclusion of Chl_{leaf}. There was a nonlinearity between the GPP estimated by BEPS-TRY and RSIF and FLUXCOM GPP, as BEPS-TRY tended to overestimate GPP at regions where FLUXCOM GPP was larger than 300 g m^{-2} yr^{-1} (Figure 6). But this overestimation of GPP by BEPS-TRY was corrected by using BEPS-Chl_{leaf} (Figure 6).

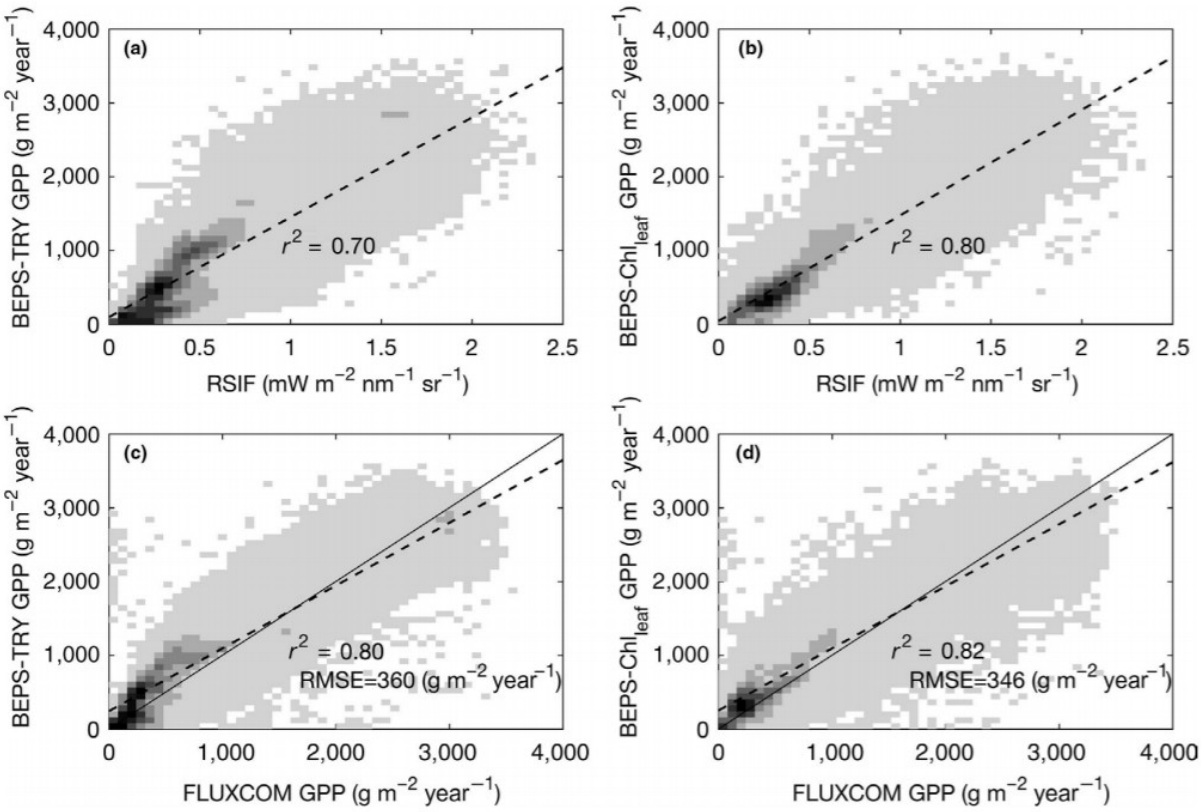

Figure 6. Validation of the spatial variability of annual gross primary production (GPP) estimated by BEPS-TRY and BEPS-Chl_{leaf} against a reconstructed SIF product (RSIF) and the FLUXCOM gridded GPP product. (a) BEPS-TRY GPP versus RSIF; (b) BEPS-Chl_{leaf} GPP versus RSIF; (c) BEPS-TRY GPP versus FLUXCOM ensemble mean GPP; and (d) BEPS-Chl_{leaf} GPP versus FLUXCOM ensemble mean GPP. Density of points is indicated by grey scale with darker colour meaning higher density. Dash lines are the linear regression line and solid lines are the 1:1 reference line

Evaluation of estimated monthly GPP with RSIF and FLUXCOM GPP showed that Chl_{leaf} effectively improved GPP estimates in most months and for some PFTs (Figure 7). Based on the correlation between estimated GPP and RSIF (Figure 7a), CRO, DBF, GRA, SAV and WET were the five PFTs that improved r^2 in most months, with the average r^2 increased 0.06. EBF, ENF, MF and SH showed decline in r^2 in most months. Meanwhile, the validation against FLUXCOM GPP (Figure 7b) confirmed the positive impacts of Chl_{leaf} in estimating GPP for CRO, DBF, GRA, SAV and WET. SH only showed increased r^2 at the beginning of the year but had decreased r^2 in most months. The comparison between estimated GPP and FLUXCOM GPP reaffirmed the negligible effect of Chl_{leaf} on EBF, but suggested considerable increases in r^2 for ENF and MF (Figure 7b), which was not found in the validation against RSIF (Figure 7a) and eddy covariance measurements (Figure 3).

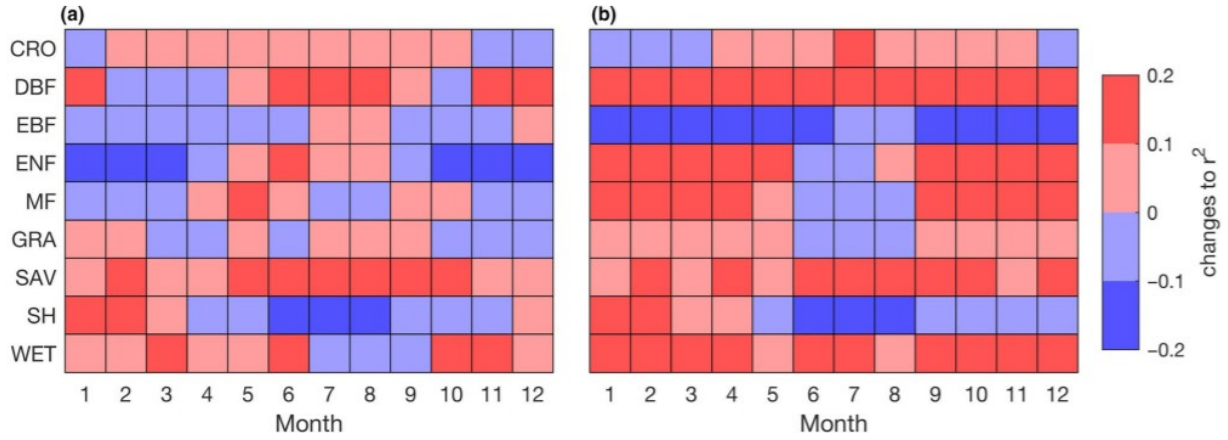

Figure 7. Evaluation of estimated monthly gross primary production (GPP) for each PFT using RSIF and FLUXCOM. (a) the increase or decrease of the correlation coefficient (r^2) between estimated GPP and RSIF after the inclusion of Chl_{leaf}; (b) the increase or decrease of the correlation coefficient (r^2) between estimated GPP and FLUXCOM after the inclusion of Chl_{leaf}. Acronyms for PFTs are CRO (croplands), DBF (deciduous broadleaf forests), EBF (evergreen broadleaf forests), ENF (evergreen needleleaf forests), MF (mixed forests), GRA (grasslands), SAV (savannas), SH (shrublands) and WET (wetlands)

4 DISCUSSION

This study presents the first use of satellite-derived, temporal-spatially continuous plant physiological information (i.e. Chl_{leaf}) to estimate GPP for globally distributed ecosystems. The inclusion of temporally and spatially explicit Chl_{leaf} in a TBM reduced the bias of estimated daily GPP by 8% and improved the temporal correlation between estimates and observations by 5% on average for 124 eddy covariance sites (555 site-years). These improvements accumulated to a 28% reduction in RMSE of annual GPP estimates, and a 14% increase in the spatial correlation between annual estimates and observations. PFTs with strong seasonal cycles (i.e. DBF, CRO, GRA, SAV and WET) demonstrated significant improvements, with up to 21% reduction in bias and up to 22% increase in temporal r^2. We also noticed mixed impacts of Chl_{leaf} on GPP estimates for SH and EBF and mostly negative impacts for ENF and MF. Based on the reduction of bias of daily GPP estimates, we found that the temporal and spatial variations of Chl_{leaf} contributed equally to the improvements of GPP estimates. Global estimation of GPP was 9 PgC lower after the inclusion of Chl_{leaf} in 2011 and better captured the variability of RSIF and FLUXCOM GPP.

4.1 Disparity in the temporal profiles of Chl_{leaf} and LAI

Our results demonstrated a wide-spread disparity in the temporal profiles of Chl_{leaf} and LAI for all PFTs (Figure 1), which has been noted by several in situ studies on some tree species (Croft et al., 2017; Croft, Chen, & Zhang, 2014a; Kodani, Awaya, Tanaka, & Matsumura, 2002). This disparity highlights an asynchrony between the physiological and the structural development of plants. The reason for this disparity remains unidentified. It is possible that Chl_{leaf} and LAI develop different temporal profiles to optimally use limited resources (i.e. light), in a way similar to some leaf traits (i.e.

nitrogen, Vc_{max}^{25}) which develop a vertical profile mimicking the gradient of solar radiation in the canopy to maximize the total carbon uptake of a whole stand (Anten, Schieving, & Werger, 1995; Field, 1983; Hirose & Werger, 1987). In addition, we noticed that the degree of the asynchrony between Chl_{leaf} and LAI varies among PFTs (Figure 1). For SH and ENF, the disparities between the temporal profiles of Chl_{leaf} and LAI were relatively small, which may justify some modelling practices to use LAI to emulate the seasonality of Vc_{max}^{25} of ENF (Luo, Chen, et al., 2018; Ryu et al., 2011). However, for most PFTs, the temporal profiles of physiological status (i.e. Chl_{leaf}) cannot be replaced by those of LAI in TBMs.

4.2 Comparison with previous studies using Chl_{leaf} to estimate GPP

The positive impact of Chl_{leaf} on GPP estimates found in our study is comparable to the results of previous site-level studies. Houborg et al. (2013) reported a 12% increase in temporal correlation (r^2) and a 24% decrease in RMSE of estimated growing season GPP after using Chl_{leaf} in the Community Land Model (Bonan et al., 2011) at a CRO site. Luo, Croft, et al. (2018) incorporated Chl_{leaf} in BEPS at a DBF site and reported a 10% increase in temporal r^2 and a 32% decrease in RMSE. In this study, we found the average improvement in the temporal r^2 for 87 site-years of CRO and 65 site-years of DBF was 22% and 9%, respectively, and their reductions in AAB, an indicator similar to RMSE, were 21% and 15% respectively (Figure 3). At the global scale, Alton (2017) used MERIS terrestrial chlorophyll index (MTCI) as a proxy for chlorophyll content to retrieve the Vc_{max}^{25} of 296 FLUXNET sites and found the inclusion of spatially and temporally varying MTCI-based Vc_{max}^{25} in JULES-SF led to a 15% decrease in annual GPP estimates on site-average. Meanwhile, our study found a 7% decrease of annual GPP across 124 sites and a 7% decrease of global GPP. Our study took a somewhat different approach than the Alton (2017) study to incorporate Chl_{leaf} into a TBM. The Alton (2017) study assumes a constant conversion rate from Chl_{leaf} to Vc_{max}^{25} for all leaves and PFTs, but several field-based studies have suggested that the Chl_{leaf}-Vc_{max}^{25} relationship is likely to change with PFTs (Croft et al., 2017; Houborg, McCabe, Cescatti, & Gitelson, 2015) and light environment (Evans, 1989a). Our result also suggests that MTCI, though widely used for carbon modelling (He et al., 2017; Yao Zhang, Xiao, et al., 2018), might not be able to capture the variability of global measured Chl_{leaf} (r^2 = 0.27) as good as our satellite-derived Chl_{leaf} product (r^2 = 0.47) (Supplementary Information, section 2). In addition, even though a site-level study has established a Chl_{leaf}-Vc_{max}^{25} relationship for C4 species and reported improved photosynthesis estimates (Houborg et al., 2013), a lack of knowledge about the global distribution of C4 species in our PFT map prohibited us from applying this relationship for global GPP estimation.

4.3 Influence of light environment on Chl_{leaf}-Vc_{max}^{25} relationship

The ratio between Chl_{leaf} and Vc_{max}^{25} can differ between sunlit and shaded leaves, with sunlit leaves showing a higher Vc_{max}^{25} to Chl_{leaf} ratio than that of shaded leaves (Evans, 1989a). It is possible that such changes also reflect the optimal distribution of the nitrogen within the canopy to maximize the whole canopy photosynthesis (Anten et al.., 1995). This difference in the Vc_{max}^{25} to Chl_{leaf} ratio between sunlit and shaded leaves is consistent with previous studies reporting Chl_{leaf} varies little under different solar irradiance (Lambers, Chapin, & Pons, 2008; Walters, 2005) while leaf nitrogen content and Vc_{max}^{25} both decrease proportionally from the top to the bottom of the canopy following radiation gradient (Hirose & Werger, 1987; Warren & Adams, 2001). In this study, we incorporate these observational patterns in an updated two-leaf upscaling scheme for BEPS (Luo, Croft, et al., 2018) in which we assume the sunlit and shaded leaves have Chl_{leaf} similar to the Chl_{leaf} of leaves on top of the canopy, and Vc_{max}^{25} of sunlit and shaded leave can be calculated based on a presumed nitrogen gradient (De Pury & Farquhar, 1997) and the Chl_{leaf}-based Vc_{max}^{25} of top leaves. The results from that site-level study have suggested that the physiological difference between sunlit and shaded leaves was effectively reproduced by this updated two-leaf scheme (Luo, Croft, et al., 2018). Although our approach assumes that leaf nitrogen content is not a robust proxy for the temporal profile of Vc_{max}^{25} (Croft et al., 2017) because of the dynamic allocation of nitrogen to photosynthetic and nonphotosynthetic components, leaf nitrogen content remains a good proxy for the vertical profile of Vc_{max}^{25} (Wilson, Baldocchi, & Hanson, 2000).

4.4 Influence of leaf age on Chl_{leaf}-Vc_{max}^{25} relationship

Our results demonstrated mixed impacts of Chl_{leaf} on the estimation of GPP for EBF and negative impacts of Chl_{leaf} for ENF and MF. These three PFTs all have evergreen species that contain leaves or needles of several age groups. Katahata, Naramoto, Kakubari, and Mukai (2007) reported that needle leaves belonging to ages of 1, 2 and 3 years showed different seasonal trends in Chl_{leaf} and Vc_{max}^{25}. Young needles had an increasing trend in Chl_{leaf} while old needles showed the opposite. Warren and Adams (2001) and Ethier et al. (2006) both found reduced photosynthetic capacity for old needles while their leaf nitrogen content is almost the same as young needles. As for EBF, a study in Amazonia demonstrated that leaf age composition explains 27% of the variation in photosynthesis, and that young leaves have higher light use efficiency than the old leaves (Wu et al., 2016). These studies indicate that leaf age is potentially another factor driving the variation in Chl_{leaf} and Vc_{max}^{25} within a canopy; however, the role of leaf age was not at all accounted for in our algorithms to derive Chl_{leaf} or Chl_{leaf}-Vc_{max}^{25} relationships. A recent study has managed to estimate leaf ages using the PLSR model driven by leaf

reflectance for some Amazonian trees (Chavana-Bryant et al., 2017), implying the possibility of deriving leaf age and its corresponding Chl_{leaf} from satellite data in the future. We suggest that a proper consideration of leaf demography and its impact on Chl_{leaf} and Vc_{max}^{25} for evergreen species is necessary to simulate GPP with Chl_{leaf} for EBF, ENF and MF.

4.5 Influence of Chl_{leaf} on fraction of absorbed photosynthetic active radiation (fAPAR)

Many leaf-level studies have found that absorptance of photosynthetic active radiation (PAR; 400-700 nm) of leaves increases with the increase of Chl_{leaf} (Evans & Poorter, 2001; Poorter et al., 2000), suggesting that Chl_{leaf} is a major factor impacting fAPAR of leaves. However, our study did not explicitly consider the impact of Chl_{leaf} on fAPAR, due to the fact that at the canopy scale Chl_{leaf} can only impact fAPAR to a small degree. The limited impact of Chl_{leaf} on canopy fAPAR was suggested by observational and model results (Daughtry, 2000; Migliavacca et al., 2017). Layers of leaves in a canopy leverage reflected and scattered solar radiation within the canopy, and subsequently render the canopy fAPAR much higher and less variable than its leaf counterpart (Croft, Chen, & Zhang, 2014b). Therefore, it is the canopy structure (i.e. LAI, clumping, leaf angle distribution) that dictates canopy fAPAR (Asner, 1998; Asner & Wessman, 1997) rather than Chl_{leaf}. A sensitivity test of our radiative transfer model shows a sevenfold increase in Chl_{leaf} only led to around 1%–5% of increase in canopy fAPAR (Croft et al., 2014b), which is negligible compared to the impact of Chl_{leaf} on Vc_{max}^{25} (i.e. sevenfold increase in Chl_{leaf} means 700% increase in Vc_{max}^{25}). The changes in Chl_{leaf} may impact the amount of APAR distributed between leaves but the total APAR for the canopy is likely not sensitive to the changes in Chl_{leaf}. It explains why most studies incorporating Chl_{leaf} in TBMs only consider the impact of Chl_{leaf} on Vc_{max}^{25} (Alton, 2017; Houborg et al., 2013; Luo, Croft, et al., 2018) and light use efficiency (Croft, Chen, Froelich, Chen, & Staebler, 2015; Croft, Chen, Zhang, et al., 2015; Houborg, Anderson, Daughtry, Kustas, & Rodell, 2011) and neglect the impact of Chl_{leaf} on APAR. However, we acknowledge that the impact of Chl_{leaf} on canopy fAPAR, though usually small, needs to be addressed in some special cases (i.e. planophile canopies) where leaf optical properties likely impact canopy fAPAR considerably.

Chlorophyll is vital to all plants on the Earth's land surface by harvesting light and transporting electrons to support the production of biochemical energy necessary to drive photosynthesis and maintaining ecosystem services. Chl_{leaf} is an essential vegetation trait that impacts the cycling of carbon, water and energy between the terrestrial biosphere and the atmosphere. We found that the inclusion of Chl_{leaf} can effectively constrain the uncertainty of modelled photosynthesis for various PFTs, particularly those with strong seasonal cycles, and provide a more realistic estimation of global GPP. We

suggest that Chl_{leaf} is a valuable leaf physiological trait to add in future TBMs to better simulate the terrestrial carbon cycle.

ACKNOWLEDGEMENTS

XL, HC, JMC and LH were supported by a Discovery Grant and a Strategic Grant from the Natural Science and Engineering Council of Canada. XL and TFK were supported by the NASA Terrestrial Ecology Program IDS Award NNH17AE86I. JMC and LH were supported by a Canadian Space Agency grant (14SUSMAPTO). We thank the Copernicus Global Land Service GEOV1 for providing global LAI. We thank Dr. Pierre Gentine for making reconstructed SIF available and Dr. Martin Jung for making FLUXCOM data available. XL thank Dr. Dennis Baldocchi from University of California, Berkeley, Dr. Sarah Finkelstein, Dr. Danny Harvey, Dr. Paul Kushner and Dr. Jane Liu from University of Toronto for the helpful comments on the paper in its thesis format. This work used eddy covariance data acquired and shared by the FLUXNET community, including these networks: AmeriFlux, AfriFlux, AsiaFlux, CarboAfrica, CarboEuropeIP, CarboItaly, CarboMont, ChinaFlux, Fluxnet-Canada, GreenGrass, ICOS, KoFlux, LBA, NECC, OzFlux-TERN, TCOS-Siberia and USCCC. The ERA-Interim reanalysis data are provided by ECMWF and processed by LSCE. The FLUXNET eddy covariance data processing and harmonization was carried out by the European Fluxes Database Cluster, AmeriFlux Management Project and Fluxdata project of FLUXNET, with the support of CDIAC and ICOS Ecosystem Thematic Center, and the OzFlux, ChinaFlux and AsiaFlux offices. The eddy covariance site used is listed in Table S1. Data and codes are available per request to the corresponding author. We appreciate the constructive comments from the two anonymous reviewers.

REFERENCES

Alton, P. B. (2017). Retrieval of seasonal Rubisco-limited photosynthetic capacity at global FLUXNET sites from hyperspectral satellite remote sensing: Impact on carbon modelling. *Agricultural and Forest Meteorology*, 232, 74– 88. https://doi.org/10.1016/j.agrformet.2016.08.001

Anav, A., Friedlingstein, P., Beer, C., Ciais, P., Harper, A., Jones, C., … Zhao, M. (2015). Spatiotemporal patterns of terrestrial grossprimary production: A review. *Reviews of Geophysics*, 53, 785– 818. https://doi.org/10.1002/2015RG000483

Anten, N. P. R., Schieving, F., & Werger, M. J. A. (1995). Patterns of light and nitrogen distribution in relation to whole canopy carbon gain in C3 and C4 mono- and dicotyledonous species. *Oecologia*, 101, 504– 513. https://doi.org/10.1007/BF00329431

Asner, G. P. (1998). Biophysical and biochemical sources of variability in canopy reflectance. *Remote Sensing of Environment*, 64(3), 234– 253. https://doi.org/10.1016/S0034-4257(98)00014-5

Asner, G. P., & Wessman, C. A. (1997). Scaling PAR absorption from the leaf to landscape level in spatially heterogeneous ecosystems. *Ecological Modelling*, 103(1), 81– 97. https://doi.org/10.1016/S0304-3800(97)00080-X

Baldocchi, D. (2008). “Breathing” of the terrestrial biosphere: Lessons learned from a global network of carbon dioxide flux measurement systems. *Australian Journal of Botany*, 56(1), 2499. https://doi.org/10.1071/BT07151

Baldocchi, D., Ryu, Y., & Keenan, T. (2016). Terrestrial Carbon Cycle Variability. *F1000Research*, 5, 2371. https://doi.org/10.12688/f1000research.8962.1

Baret, F., Weiss, M., Lacaze, R., Camacho, F., Makhmara, H., Pacholcyzk, P., & Smets, B. (2013). GEOV1: LAI, FAPAR essential climate variables and FCOVER global time series capitalizing over existing products. Part 1: Principles of development and production. *Remote Sensing of Environment*, 137, 299– 309. https://doi.org/10.1016/j.rse.2012.12.027

Barnes, M. L., Breshears, D. D., Law, D. J., van Leeuwen, W. J. D., Monson, R. K., Fojtik, A. C., … Moore, D. J. P. (2017). Beyond greenness: Detecting temporal changes in photosynthetic capacity with hyperspectral reflectance data. *PLoS ONE*, 12(12), 2499– 17. https://doi.org/10.1371/journal.pone.0189539

Beer, C., Reichstein, M., Tomelleri, E., Ciais, P., Jung, M., Carvalhais, N., … Papale, D. (2010). Terrestrial gross carbon dioxide uptake: Global distribution and covariation with climate. *Science*, 329(5993), 834– 838. https://doi.org/10.1126/science.1184984

Bonan, G. B., Lawrence, P. J., Oleson, K. W., Levis, S., Jung, M., Reichstein, M., … Swenson, S. C. (2011). Improving canopy processes in the Community Land Model version 4 (CLM4) using global flux fields empirically inferred from FLUXNET data. *Journal of Geophysical Research*, 116(G2), G02014. https://doi.org/10.1029/2010JG001593

Bond-Lamberty, B., & Thomson, A. (2010). Temperature-associated increases in the global soil respiration record. *Nature*, 464(7288), 579– 582. https://doi.org/10.1038/nature08930

Chavana-Bryant, C., Malhi, Y., Wu, J., Asner, G. P., Anastasiou, A., Enquist, B. J., … Gerard, F. F. (2017). Leaf aging of Amazonian canopy trees as revealed by spectral and physiochemical measurements. *New Phytologist*, 214(3), 1049– 1063. https://doi.org/10.1111/nph.13853

Chen, J. M., Deng, F., & Chen, M. (2006). Locally adjusted cubic-spline capping for reconstructing seasonal trajectories of a satellite-derived surface parameter. *IEEE Transactions on Geoscience and Remote Sensing*, 44(8), 2230– 2237. https://doi.org/10.1109/TGRS.2006.872089

Chen, J. M., & Leblanc, S. G. (1997). A four-scale bidirectional reflectance model based on canopy architecture. *IEEE Transactions on Geoscience and Remote Sensing*, 35(5), 1316– 1337. Retrieved from http://ieeexplore.ieee.org/lpdocs/epic03/wrapper.htm?arnumber=628798

Chen, J., Liu, J., Cihlar, J., & Goulden, M. (1999). Daily canopy photosynthesis model through temporal and spatial scaling for remote sensing applications. *Ecological Modelling*, 124(2–3), 99– 119. https://doi.org/10.1016/S0304-3800(99)00156-8

Chen, J. M., Rich, P. M., Gower, S. T., Norman, J. M., & Plummer, S. (1997). Leaf area index of boreal forests: Theory, techniques, and measurements. *Journal of Geophysical Research: Atmospheres*, 102(D24), 29429– 29443. https://doi.org/10.1029/97JD01107

Croft, H., Chen, J. M., Froelich, N. J., Chen, B., & Staebler, R. M. (2015). Seasonal controls of canopy chlorophyll content on forest carbon uptake: Implications for GPP modeling. *Journal of Geophysical Research Biogeosciences*, 120(8), 1576– 1586. https://doi.org/10.1002/2015JG002980

Croft, H., Chen, J. M., Luo, X., Bartlett, P., Chen, B., & Staebler, R. M. (2017). Leaf chlorophyll content as a proxy for leaf photosynthetic capacity. *Global Change Biology*, 23(9). https://doi.org/10.1111/gcb.13599

Croft, H., Chen, J. M., Mo, G., Luo, S., Luo, X., Arabian, J., … Bonal, D. (Under Review). Global distribution of leaf chlorophyll content. *Remote Sensing of Environment*.

Croft, H., Chen, J. M., & Zhang, Y. (2014a). Temporal disparity in leaf chlorophyll content and leaf area index across a growing season in a temperate deciduous forest. *International Journal of Applied Earth Observation and Geoinformation*, 33(1), 312– 320. https://doi.org/10.1016/j.jag.2014.06.005

Croft, H., Chen, J. M., & Zhang, Y. (2014b). The applicability of empirical vegetation indices for determining leaf chlorophyll content over different leaf and canopy structures. *Ecological Complexity*, 17, 119– 130. https://doi.org/10.1016/j.ecocom.2013.11.005

Croft, H., Chen, J. M., Zhang, Y., & Simic, A. (2013). Modelling leaf chlorophyll content in broadleaf and needle leaf canopies from ground, CASI, Landsat TM 5 and MERIS reflectance data. *Remote Sensing of Environment*, 133, 128– 140. https://doi.org/10.1016/j.rse.2013.02.006

Croft, H., Chen, J. M., Zhang, Y., Simic, A., Noland, T. L., Nesbitt, N., & Arabian, J. (2015). Evaluating leaf chlorophyll content prediction from multispectral remote sensing data within a physically-based modelling framework. *ISPRS Journal of Photogrammetry and Remote Sensing*, 102, 85– 95. https://doi.org/10.1016/j.isprsjprs.2015.01.008

Curran, P. J., & Steele, C. M. (2005). MERIS: The re-branding of an ocean sensor. *International Journal of Remote Sensing*, 26(9), 1781– 1798. https://doi.org/10.1080/01431160412331330275

Daughtry, C. (2000). Estimating corn leaf chlorophyll concentration from leaf and canopy reflectance. *Remote Sensing of Environment*, 74(2), 229– 239. https://doi.org/10.1016/S0034-4257(00)00113-9

De Pury, D. G. G., & Farquhar, G. D. (1997). Simple scaling of photosynthesis from leaves to canopies without the errors of big-leaf models. *Plant, Cell and Environment*, 20(5), 537– 557. https://doi.org/10.1111/j.1365-3040.1997.00094.x

Dechant, B., Cuntz, M., Vohland, M., Schulz, E., & Doktor, D. (2017). Estimation of photosynthesis traits from leaf reflectance spectra: Correlation to nitrogen content as the dominant mechanism. *Remote Sensing of Environment*, 196, 279– 292. https://doi.org/10.1016/j.rse.2017.05.019

Ethier, G. J., Livingston, N. J., Harrison, D. L., Black, T. A., & Moran, J. A. (2006). Low stomatal and internal conductance to CO2 versus Rubisco deactivation as determinants of the photosynthetic decline of ageing evergreen leaves. *Plant, Cell and Environment*, 29(12), 2168– 2184. https://doi.org/10.1111/j.1365-3040.2006.01590.x

Evans, J. (1989a). Partitioning of nitrogen between and within leaves grown under different irradiances. *Australian Journal of Plant Physiology*, 16(6), 533. https://doi.org/10.1071/PP9890533

Evans, J. (1989b). Photosynthesis and nitrogen relationships in leaves of C3 plants. *Oecologia*, 78(1), 9– 19. https://doi.org/10.1007/BF00377192

Evans, J. R., & Poorter, H. (2001). Photosynthetic acclimation of plants to growth irradiance: the relative importance of specific leaf area and nitrogen partitioning in maximizing carbon gain, *Plant, Cell & Environment*, 24, 755– 767.

Farquhar, G. D., von Caemmerer, S., & Berry, J. A. (1980). A biochemical model of photosynthetic CO2 assimilation in leaves of C3 species. *Planta*, 149(1), 78– 90. https://doi.org/10.1007/BF00386231

Field, C. (1983). Allocating leaf nitrogen for the maximization of carbon gain: Leaf age as a control on the allocation program. *Oecologia*, 56(2), 341– 347. https://doi.org/10.1007/BF00379710

Frankenberg, C., Fisher, J. B., Worden, J., Badgley, G., Saatchi, S. S., Lee, J. E. … Yokota, T. (2011). New global observations of the terrestrial carbon cycle from GOSAT: Patterns of plant fluorescence with gross primary

productivity, *Geophysical Research Letters*, 38, 2499– 6. https://doi.org/10.1029/2011GL048738

Friedl, M. A., Sulla-Menashe, D., Tan, B., Schneider, A., Ramankutty, N., Sibley, A., & Huang, X. (2010). MODIS Collection 5 global land cover: Algorithm refinements and characterization of new datasets. *Remote Sensing of Environment*, 114(1), 168– 182. https://doi.org/10.1016/j.rse.2009.08.016

Gentine, P., & Alemohammad, S. H. (2018). Reconstructed solar-induced fluorescence: A machine learning vegetation product based on modis surface reflectance to reproduce GOME-2 solar-induced fluorescence. *Geophysical Research Letters*, 45(7), 3136– 3146. https://doi.org/10.1002/2017GL076294

Gonsamo, A., Chen, J. M., Price, D. T., Kurz, W. A., Liu, J., Boisvenue, C., … Chang, K.-H. (2013). Improved assessment of gross and net primary productivity of Canada's landmass. *Journal of Geophysical Research: Biogeosciences*, 118(4), 1546– 1560. https://doi.org/10.1002/2013JG002388

Grant, R. F., Zhang, Y., Yuan, F., Wang, S., Hanson, P. J., Gaumont-Guay, D., … Arain, A. (2006). Intercomparison of techniques to model water stress effects on CO2 and energy exchange in temperate and boreal deciduous forests. *Ecological Modelling*, 196(3–4), 289– 312. https://doi.org/10.1016/j.ecolmodel.2006.02.035

Guanter, L., Zhang, Y., Jung, M., Joiner, J., Voigt, M., Berry, J. A., … Griffis, T. J. (2014). Global and time-resolved monitoring of crop photosynthesis with chlorophyll fluorescence. *Proceedings of the National Academy of Sciences*, 111(14), E1327– E1333. https://doi.org/10.1073/pnas.1320008111

He, L., Chen, J. M., Croft, H., Gonsamo, A., Luo, X., Liu, J., Liu, Y. (2017). Nitrogen availability dampens the positive impacts of CO_2 fertilization on terrestrial ecosystem carbon and water cycles. *Geophysical Research Letters*, 44(22). https://doi.org/10.1002/2017GL075981

He, L., Chen, J. M., Gonsamo, A., Luo, X., Wang, R., Liu, Y., & Liu, R. (2018). Changes in the shadow: The shifting role of shaded leaves in global carbon and water cycles under climate change. *Geophysical Research Letters*, 82(3), 387. https://doi.org/10.1029/2018GL077560

He, L., Chen, J. M., Pisek, J., Schaaf, C. B., & Strahler, A. H. (2012). Global clumping index map derived from the MODIS BRDF product. *Remote Sensing of Environment*, 119, 118– 130. https://doi.org/10.1016/j.rse.2011.12.008

Hikosaka, K., & Terashima, I. (1996). Nitrogen partitioning among photosynthetic components and its consequenses in sun and shade plants. *Functional Ecology*, 10(3), 335– 343. https://doi.org/10.2307/2390281

Hirose, T., Werger, M. J. A. (1987). Maximizing dialy canopy photosynthesis with respect to the leaf nitrogen allocation pattern in the canopy. *Oecologia*, 72(4), 520– 526. https://doi.org/10.1007/BF00378977

Houborg, R., Anderson, M. C., Daughtry, C. S. T., Kustas, W. P., & Rodell, M. (2011). Using leaf chlorophyll to parameterize light-use-efficiency within a thermal-based carbon, water and energy exchange model. *Remote Sensing of Environment*, 115(7), 1694– 1705. https://doi.org/10.1016/j.rse.2011.02.027

Houborg, R., Cescatti, A., Migliavacca, M., & Kustas, W. P. (2013). Satellite retrievals of leaf chlorophyll and photosynthetic capacity for improved modeling of GPP. *Agricultural and Forest Meteorology*, 177, 10– 23. https://doi.org/10.1016/j.agrformet.2013.04.006

Houborg, R., McCabe, M., Cescatti, A., Gao, F., Schull, M., & Gitelson, A. (2015). Joint leaf chlorophyll content and leaf area index retrieval from Landsat data using a regularized model inversion system (REGFLEC). *Remote Sensing of Environment*, 159, 203– 221. https://doi.org/10.1016/j.rse.2014.12.008

Houborg, R., McCabe, M. F., Cescatti, A., & Gitelson, A. A. (2015). Leaf chlorophyll constraint on model simulated gross primary productivity in agricultural systems. *International Journal of Applied Earth Observation and Geoinformation*, 43, 160– 176. https://doi.org/10.1016/j.jag.2015.03.016

Jacquemoud, S., & Baret, F. (1990). PROSPECT: A model of leaf optical properties spectra. *Remote Sensing of Environment*, 34(2), 75– 91. https://doi.org/10.1016/0034-4257(90)90100-Z

Jacquemoud, S., & Ustin, S. L. (2001). Leaf optical properties: a state of the art. *Proceeding 8th International Symposium Physical Measurements & Signatures in Remote Sensing*, January, 223– 232. https://doi.org/10.1017/CBO9781107415324.004

Joiner, J., Yoshida, Y., Vasilkov, A. P., Yoshida, Y., Corp, L. A., & Middleton, E. M. (2011). First observations of global and seasonal terrestrial chlorophyll fluorescence from space. *Biogeosciences*, 8(3), 637– 651. https://doi.org/10.5194/bg-8-637-2011

Jung, M., Reichstein, M., Schwalm, C. R., Huntingford, C., Sitch, S., Ahlström, A., … Zeng, N. (2017). Compensatory water effects link yearly global land CO_2 sink changes to temperature. *Nature*, 541(7638), 516– 520. https://doi.org/10.1038/nature20780

Katahata, S. I., Naramoto, M., Kakubari, Y., & Mukai, Y. (2007). Seasonal changes in photosynthesis and nitrogen allocation in leaves of different ages in evergreen understory shrub Daphniphyllum humile. *Trees - Structure and Function*, 21(6), 619– 629. https://doi.org/10.1007/s00468-007-0155-x

Kattge, J., Knorr, W., Raddatz, T., & Wirth, C. (2009). Quantifying photosynthetic capacity and its relationship to leaf nitrogen content for global-scale terrestrial biosphere models. *Global Change Biology*, 15(4), 976– 991. https://doi.org/10.1111/j.1365-2486.2008.01744.x

Keenan, T. F., & Williams, C. A. (2018). The Terrestrial Carbon Sink. *Annual Review of Environment and Resources*, 43(1), 219– 243. https://doi.org/10.1146/annurev-environ-102017-030204

Kodani, E., Awaya, Y., Tanaka, K., & Matsumura, N. (2002). Seasonal patterns of canopy structure, biochemistry and spectral reflectance in a broad-leaved deciduous Fagus crenata canopy. *Forest Ecology and Management*, 167(1– 3), 233– 249. https://doi.org/10.1016/S0378-1127(01)00701-0

Kokaly, R. F., Asner, G. P., Ollinger, S. V., Martin, M. E., & Wessman, C. A. (2009). Characterizing canopy biochemistry from imaging spectroscopy and its application to ecosystem studies. *Remote Sensing of Environment*, 113(Suppl. 1), S78– S91. https://doi.org/10.1016/j.rse.2008.10.018

Kuusk, A. (2018). *3.03 - Canopy radiative transfer modeling A2 - Liang, Shunlin BT - comprehensive remote sensing* (pp. 9– 22). Oxford: Elsevier. https://doi.org/10.1016/B978-0-12-409548-9.10534-2

Lambers, H., Chapin, F. S., & Pons, T. L. (2008). *Plant physiological ecology*. New York, NY: Springer. https://doi.org/10.1007/978-0-387-78341-3

Le Quéré, C., Andrew, R. M., Friedlingstein, P., Sitch, S., Pongratz, J., Manning, A. C., Zhu, D. (2017). Global carbon budget 2017. *Earth System Science Data Discussions*, (November), 2499– 79. https://doi.org/10.5194/essd-2017-123

Li, W., Ciais, P., Wang, Y., Yin, Y. i., Peng, S., Zhu, Z., … Piao, S. (2018). Recent changes in global photosynthesis and terrestrial ecosystem respiration constrained from multiple observations. *Geophysical Research Letters*, 45(2), 1058– 1068. https://doi.org/10.1002/2017GL076622

Li, X., Xiao, J., & He, B. (2018). Chlorophyll fluorescence observed by OCO-2 is strongly related to gross primary productivity estimated from flux towers in temperate forests. *Remote Sensing of Environment*, 204, 659– 671. https://doi.org/10.1016/j.rse.2017.09.034

Liu, X., Guanter, L., Liu, L., Damm, A., Malenovský, Z., Rascher, U., Gastellu-Etchegorry, J. P. (2018). Downscaling of solar-induced chlorophyll fluorescence from canopy level to photosystem level using a random forest model. *Remote Sensing of Environment*, 9, https://doi.org/10.1016/j.rse.2018.05.035

Luo, X., Chen, J. M., Liu, J., Black, T. A., Croft, H., Staebler, R., … McCaughey, H. (2018). Comparison of big-leaf, two-big-leaf, and two-leaf upscaling schemes for evapotranspiration estimation using coupled carbon-water

modeling. *Journal of Geophysical Research: Biogeosciences*, 123(1), 207– 225. https://doi.org/10.1002/2017JG003978

Luo, X., Croft, H., Chen, J. M., Bartlett, P., Staebler, R., & Froelich, N. (2018). Incorporating leaf chlorophyll content into a two-leaf terrestrial biosphere model for estimating carbon and water fluxes at a forest site. *Agricultural and Forest Meteorology*, 248(September 2017), 156– 168. https://doi.org/10.1016/j.agrformet.2017.09.012

Migliavacca, M., Perez-Priego, O., Rossini, M., El-Madany, T. S., Moreno, G., van der Tol, C., … Reichstein, M. (2017). Plant functional traits and canopy structure control the relationship between photosynthetic CO2 uptake and far-red sun-induced fluorescence in a Mediterranean grassland under different nutrient availability. *New Phytologist*, 214(3), 1078– 1091. https://doi.org/10.1111/nph.14437

Misson, L., Tu, K. P., Boniello, R. A., & Goldstein, A. H. (2006). Seasonality of photosynthetic parameters in a multi-specific and vertically complex forest ecosystem in the Sierra Nevada of California. *Tree Physiology*, 26(6), 729– 741. https://doi.org/10.1093/treephys/26.6.729

Musavi, T., Migliavacca, M., Reichstein, M., Kattge, J., Wirth, C., Black, T. A., … Mahecha, M. D. (2017). Stand age and species richness dampen interannual variation of ecosystem-level photosynthetic capacity. *Nature Ecology & Evolution*, 1, 48. https://doi.org/10.1038/s41559-016-0048

Pastorello, G., Papale, D., Chu, H., Trotta, C., Agarwal, D., Canfora, E., … Torn, M. (2017). A New Data Set to Keep a Sharper Eye on Land-Air Exchanges. *Eos*, 98, https://doi.org/10.1029/2017EO071597

Piao, S., Sitch, S., Ciais, P., Friedlingstein, P., Peylin, P., Wang, X., … Zeng, N. (2013). Evaluation of terrestrial carbon cycle models for their response to climate variability and to CO 2 trends. *Global Change Biology*, 19(7), 2117– 2132. https://doi.org/10.1111/gcb.12187

Poorter, L., Kwant, R., Hernández, R., & Medina, E. (2000). Leaf optical properties in Venezuelan cloud forest trees, *Tree Physiology*, 20(8), 519– 526.

Porcar-Castell, A., Tyystjärvi, E., Atherton, J., van der Tol, C., Flexas, J., Pfündel, E. E., … Berry, J. A. (2014). Linking chlorophyll a fluorescence to photosynthesis for remote sensing applications: Mechanisms and challenges. *Journal of Experimental Botany*, 65(15), 4065– 4095. https://doi.org/10.1093/jxb/eru191

Rast, M., Bezy, J. L., & Bruzzi, S. (1999). The ESA medium resolution imaging spectrometer MERIS a review of the instrument and its mission. *International Journal of Remote Sensing*, 20(9), 1681– 1702. https://doi.org/10.1080/014311699212416

Reichstein, M., Falge, E., Baldocchi, D., Papale, D., Aubinet, M., Berbigier, P., … Valentini, R. (2005). On the separation of net ecosystem exchange into

assimilation and ecosystem respiration: Review and improved algorithm. *Global Change Biology*, 11(9), 1424– 1439. https://doi.org/10.1111/j.1365-2486.2005.001002.x

Ryu, Y., Baldocchi, D. D., Kobayashi, H., van Ingen, C., Li, J., Black, T. A., … Roupsard, O. (2011). Integration of MODIS land and atmosphere products with a coupled-process model to estimate gross primary productivity and evapotranspiration from 1 km to global scales. *Global Biogeochemical Cycles*, 25(4), GB4017. https://doi.org/10.1029/2011GB004053

Schaefer, K., Schwalm, C. R., Williams, C., Arain, M. A., Barr, A., Chen, J. M., … Zhou, X. (2012). A model-data comparison of gross primary productivity: Results from the North American Carbon Program site synthesis. *Journal of Geophysical Research*, 117(G3), G03010. https://doi.org/10.1029/2012JG001960

Serbin, S. P., Singh, A., Desai, A. R., Dubois, S. G., Jablonski, A. D., Kingdon, C. C., … Townsend, P. A. (2015). Remotely estimating photosynthetic capacity, and its response to temperature, in vegetation canopies using imaging spectroscopy. *Remote Sensing of Environment*, 167, 78– 87. https://doi.org/10.1016/j.rse.2015.05.024

Simic, A., Chen, J. M., & Noland, T. L. (2011). Retrieval of forest chlorophyll content using canopy structure parameters derived from multi-angle data: The measurement concept of combining nadir hyperspectral and off-nadir multispectral data. *International Journal of Remote Sensing*, 32(20), 5621– 5644. https://doi.org/10.1080/01431161.2010.507257

Singh, A., Serbin, S. P., McNeil, B. E., Kingdon, C. C., & Townsend, P. A. (2015). Imaging spectroscopy algorithms for mapping canopy foliar chemical and morphological traits and their uncertainties. *Ecological Applications*, 25(8), 2180– 2197. https://doi.org/10.1890/14-2098.1

Sitch, S., Friedlingstein, P., Gruber, N., Jones, S. D., Doney, S. C., Graven, H., … Myneni, R. (2015). Recent trends and drivers of regional sources and sinks of carbon, *Biogeosciences*, 12, 653– 679. https://doi.org/10.5194/bg-12-653-2015

Stinziano, J. R., Morgan, P. B., Lynch, D. J., Saathoff, A. J., McDermitt, D. K., & Hanson, D. T. (2017). The rapid A-Ciresponse: Photosynthesis in the phenomic era. *Plant Cell and Environment*, 40(8), 1256– 1262. https://doi.org/10.1111/pce.12911

Thornton, P. E., & Zimmermann, N. E. (2007). An improved canopy integration scheme for a Land Surface Model with prognostic canopy structure. *Journal of Climate*, 20(15), 3902– 3923. https://doi.org/10.1175/JCLI4222.1

Verhoef, W. (1984). Light scattering by leaf layers with applications to canopy reflectance modelling: The SAIL model. *Remote Sensing of Environment*, 16, 125– 141.

Walker, A. P., Beckerman, A. P., Gu, L., Kattge, J., Cernusak, L. A., Domingues, T. F., … Woodward, F. I. (2014). The relationship of leaf photosynthetic traits - V cmax and J max - to leaf nitrogen, leaf phosphorus, and specific leaf area: A meta-analysis and modeling study. *Ecology and Evolution*, 4(16), 3218– 3235. https://doi.org/10.1002/ece3.1173

Walker, A. P., Quaife, T., van Bodegom, P. M., De Kauwe, M. G., Keenan, T. F., Joiner, J., … Woodward, F. I. (2017). The impact of alternative trait-scaling hypotheses for the maximum photosynthetic carboxylation rate (Vcmax) on global gross primary production. *New Phytologist*, 215(4), 1370– 1386. https://doi.org/10.1111/nph.14623

Walters, R. G. (2005). Towards an understanding of photosynthetic acclimation. *Journal of Experimental Botany*, 56(411), 435– 447. https://doi.org/10.1093/jxb/eri060

Wang, Q., Tenhunen, J., Falge, E., Bernhofer, C., Granier, A., & Vesala, T. (2004). Simulation and scaling of temporal variation in gross primary production for coniferous and deciduous temperate forests. *Global Change Biology*, 10(1), 37– 51. https://doi.org/10.1111/j.1365-2486.2003.00716.x

Wang, Z., Skidmore, A. K., Darvishzadeh, R., & Wang, T. (2018). Agricultural and Forest Meteorology Mapping forest canopy nitrogen content by inversion of coupled leaf-canopy radiative transfer models from airborne hyperspectral imagery. *Agricultural and Forest Meteorology*, 253–254(August 2017), 247– 260. https://doi.org/10.1016/j.agrformet.2018.02.010

Warren, C. R., & Adams, M. A. (2001). Distribution of N, Rubisco and photosynthesis in Pinus pinaster and acclimation to light. *Plant, Cell and Environment*, 24(6), 597– 609. https://doi.org/10.1046/j.1365-3040.2001.00711.x

Wilson, K. B., Baldocchi, D. D., & Hanson, P. J. (2000). Spatial and seasonal variability of photosynthetic parameters and their relationship to leaf nitrogen in a deciduous forest. *Tree Physiolog*, 20(9), 565– 578. https://doi.org/10.1093/treephys/20.9.565

Wu, J., Albert, L. P., Lopes, A. P., Restrepo-Coupe, N., Hayek, M., Wiedemann, K. T., … Saleska, S. R. (2016). Leaf development and demography explain photosynthetic seasonality in Amazon evergreen forests. *Science*, 351(6276), 972– 976. https://doi.org/10.1126/science.aad5068. http://science.sciencemag.org/content/351/6276/972.abstract

Wullschleger, S. D. (1993). Biochemical limitations to carbon assimilation in C 3 plants—A retrospective analysis of the A/C i curves from 109 species. *Journal of Experimental Botany*, 44(5), 907– 920. https://doi.org/10.1093/jxb/44.5.907

Xu, L., & Baldocchi, D. D. (2003). Seasonal trends in photosynthetic parameters and stomatal conductance of blue oak (Quercus douglasii) under prolonged summer drought and high temperature. *Tree Physiology*, 23(13), 865– 877. https://doi.org/10.1093/treephys/23.13.865

Yang, H., Yang, X. i., Zhang, Y., Heskel, M. A., Lu, X., Munger, J. W., … Tang, J. (2017). Chlorophyll fluorescence tracks seasonal variations of photosynthesis from leaf to canopy in a temperate forest. *Global Change Biology*, 23(7), 2874– 2886. https://doi.org/10.1111/gcb.13590

Yang, K., Ryu, Y., Dechant, B., Berry, J. A., Hwang, Y., Jiang, C., … Yang, X. I. (2018). Sun-induced chlorophyll fluorescence is more strongly related to absorbed light than to photosynthesis at half-hourly resolution in a rice paddy. *Remote Sensing of Environment*, 216(February), 658– 673. https://doi.org/10.1016/J.RSE.2018.07.008

Yang, P., & van der Tol, C. (2018). Linking canopy scattering of far-red sun-induced chlorophyll fluorescence with reflectance. *Remote Sensing of Environment*, 209, 456– 467. https://doi.org/10.1016/j.rse.2018.02.029

Zhang, Y., Chen, J. M., Miller, J. R., & Noland, T. L. (2008). Leaf chlorophyll content retrieval from airborne hyperspectral remote sensing imagery. *Remote Sensing of Environment*, 112(7), 3234– 3247. https://doi.org/10.1016/j.rse.2008.04.005

Zhang, Y., Guanter, L., Berry, J. A., Joiner, J., van der Tol, C., Huete, A., … Köhler, P. (2014). Estimation of vegetation photosynthetic capacity from space-based measurements of chlorophyll fluorescence for terrestrial biosphere models. *Global Change Biology*, 20(12), 3727– 3742. https://doi.org/10.1111/gcb.12664

Zhang, Y., Guanter, L., Berry, J. A., van der Tol, C., Yang, X., Tang, J., & Zhang, F. (2016). Model-based analysis of the relationship between sun-induced chlorophyll fluorescence and gross primary production for remote sensing applications. *Remote Sensing of Environment*, 187, 145– 155. https://doi.org/10.1016/j.rse.2016.10.016

Zhang, Y., Guanter, L., Joiner, J., Song, L., & Guan, K. (2018). Spatially-explicit monitoring of crop photosynthetic capacity through the use of space-based chlorophyll fluorescence data. *Remote Sensing of Environment*, 210(March), 362– 374. https://doi.org/10.1016/j.rse.2018.03.031

Zhang, Y., Xiao, X., Wolf, S., Wu, J., Wu, X., Gioli, B., … Ardö, J. (2018). Spatio-temporal convergence of maximum daily light-use efficiency based on radiation absorption by canopy chlorophyll. *Geophysical Research Letters*, 45(8), 3508– 3519. https://doi.org/10.1029/2017GL076354

Zhao, M., Heinsch, F. A., Nemani, R. R., & Running, S. W. (2005). Improvements of the MODIS terrestrial gross and net primary

production global data set. *Remote Sensing of Environment*, 95(2), 164– 176. https://doi.org/10.1016/j.rse.2004.12.011

Zhou, S., Medlyn, B., Sabaté, S., Sperlich, D., Prentice, I. C., & Whitehead, D. (2014). Short-term water stress impacts on stomatal, mesophyll and biochemical limitations to photosynthesis differ consistently among tree species from contrasting climates. *Tree Physiology*, 34(10), 1035– 1046. https://doi.org/10.1093/treephys/tpu072